VARIATION OF NUCLEAR RADII IN THE DRIP LINE REGIONS

M. Beiner and R.J. Lombard

Institut de Physique Nucléaire, Division de Physique Théorique*,
91406-Orsay-France

D. Mas

Laboratoire de Physique, Faculté des Sciences d'Orléans
45045-Orléans Cedex-France

1. Introduction

The energy density method used in the present work originates from the Kohn's density functional approach [1] . In its earliest formulation, the Kohn's theorem says that the total energy of a fermion system can be written under the form of a functional of the density,

$$E_{tot} = E[\rho] \quad , \tag{1}$$

subject to the constraint that

$$\int \rho(r) d^3r = A \quad , \tag{2}$$

where A represents the particle number. The ground state properties are then obtained by minimizing E_{tot} with respect to $\rho(r)$. The ground state density $\rho_0(r)$ determines not only the total energy of the system but also any observable directly related to it. For instance, it gives the average size of the system, usually taken as the r.m.s. radius. Consequently, in the functional method, checking the particle distributions appears as important as checking the binding energies when testing the validity of a particular functional. Conversely, in a idealized case, if a functional reproduces binding energies accurately, it must yield accurate ground state densities.

Adapting the method to nuclei, a functional has been constructed by considering a density dependent effective interaction (derived in connection with nuclear matter properties) and a ground state wave function taken as the product of proton and neutron unprojected B.C.S.-wave functions. The field variables are constituted by single particle orbitals and their occupation numbers. The minimization procedure leads to a system of Hartree-Fock-Bogoliubov type coupled equations. By neglecting the variational derivatives of the pairing correlation energy with respect to the single particle orbitals in the field equations (which turns out to be a reasonable approximation), the system reduces to Hartree-Fock-BCS equations, which can be solved rather easily by iterations. The gap matrix is calculated by means of a simple effective interaction derived from the Hamada-Johnston potential. Details concerning the basic equations can be found in ref. 2].

*Laboratoire associé au C.N.R.S.

The energy density method has been used to calculate the ground state properties of about 2500 spherical nuclei inside the drip lines for $N \leqslant 88 (\forall Z)$ and $Z \leqslant 54$ $(\forall N)$ with few exceptions around Z=82 and N=126. Results concerning the binding energies have already been discussed [3]. To fix ideas we recall that for the known spherical nuclei, the average difference between calculated and measured binding energies is of about -2.5 Mev with a mean quadratic deviation of 1.7 Mev.

In the case of particle distributions, the main problem consists in extracting useful informations from experimental data, unless model independent analyses exist. In order to avoid a tedious discussion, which stands outside the scope of the present paper, we shall simply quote the following results :

For stable spherical nuclei, the electron elastic differential cross sections calculated by using our self-consistent charge distributions are in good agreement with available experimental data up to momentum transfers of about $2fm^{-1}$. The charge radii agree with experimental values [4] within 1-2%. Similarly the proton and neutron densities have been used successfully to calculate hadron scattering cross sections (mainly elastic scattering) [5]. This general agreement, which is found roughly from ^{16}O up to ^{208}Pb [6], guaranties that the model is free from particular distorsions and gives us confidence when extrapolating it to unstable nuclei.

In what is following, we shall be concerned with the predictions of the energy density method with respect to the nuclear sizes (r.m.s. radii). It is known that the commonly accepted $A^{1/3}$-type laws are only approximative and deviations are expected to grow significantly as one goes away from the β-stability region. Particular attention will be payed to the variation of nuclear radii in the drip line regions. Implications of the resulting large total Coulomb energy variations between neighbouring nuclei will be emphasized.

2. Properties of the calculated nucleon distributions

2.1 Proton distributions of stable nuclei

The experimental r.m.s. charge radius, r_c, is accurately known for many stable even

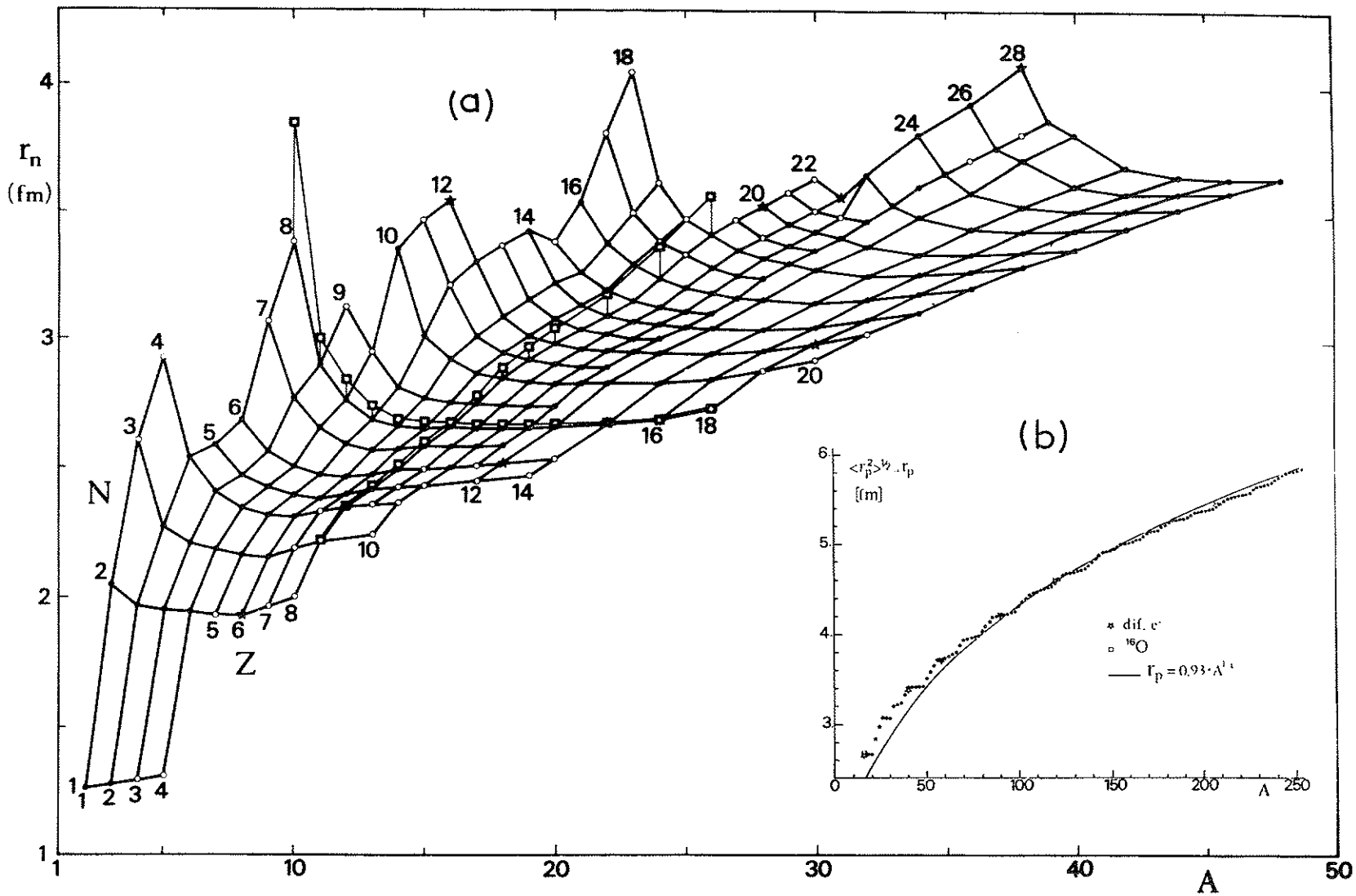

Fig.1 (a) Root-mean-square radius, r_n, of the calculated neutron distribution of light spherical nuclei plotted as function of Z and N. The meaning of the graphical symbols is described in the caption for fig.4 (circles and stars) and in the text (open squares).

(b) Variation against A of the r.m.s. radius, r_p, of the proton distribution of even stable nuclei (see text).

nuclei distributed along the valley of β-stability. A good estimate of the r.m.s. proton radius, r_p, can then be obtained by using the following simple relation

$$r_p = (r_c^2 - 0.64)^{1/2} \qquad (3)$$

based upon the assumption of a gaussian charge distribution of the proton.

The variation of r_p against A is given in the right lower part of Fig.1. The calculated values correspond to even nuclei lying on a step line which connects alternatively isotope and isotone series. Each isotope (isotone) series contains all the nuclei for which the masses have been measured [7]. This step line follows on the average the valley of β-stability (starting at ^{16}O and ending at ^{254}Fm) and allows to study separately the theoretical effect on the proton radius of the addition of pairs of protons (black stars) and of pairs of neutrons (black circles). We have also plotted the experimental proton radius (open stars) of ^{16}O, ^{40}Ca, ^{58}Ni, ^{90}Zr, ^{120}Sn and ^{208}Pb.

This plot shows clearly that

i) the agreement between experimental and calculated r.m.s. proton radii is very good ;

ii) the average behaviour of the calculated proton radius along the valley of β-stability is almost consistent with a $A^{1/3}$-law. However such a law underestimates r_p in the case of light nuclei and overestimates it slightly in the heavy ones ;

iii) the proton radius of isotopes (isotones) increases less (more) rapidly that the prediction of the average $A^{1/3}$-law. This is in qualitative agreement with the experimental data [4].

2.2 Deviations of the nuclear sizes from $A^{1/3}$-laws

It is interesting to check if property iii) holds on a larger scale and if a similar, symmetrical situation occurs for the neutron r.m.s. radius r_n. The study of the variations of the nuclear radii of even spherical nuclei ranging from one drip line to the other will therefore bring significant informations.

We have found that the two calculated functions of two integer variables $r_p(Z,N)$ and $r_n(Z,N)$ cannot be approximated with an acceptable accuracy by simple $A^{1/3}$-laws, even in relatively small domains of the arguments Z,N. In particular, for a given value of A, r_p as well as r_n spreads out by sizeable amounts as one proceeds from the proton to the neutron drip line.

The results summarized in Table 1, which concern ten series of even isobars, give a first illustration of this finding. They are briefly described in the following three paragraphs :

i) Except for ^{140}Er, all the proton-rich extreme isobars $(Z,N)^{(p)}$ (see caption for Table 1) are unstable against the emission of one proton, whereas the large majority of the neutron-rich extreme isobars $(Z,N)^{(n)}$ are stable against the emission of a single neutron.

ii) The pairs of tabulated isobars are mirror nuclei only for A=10. In this case, we note that Δr_p is significantly larger than Δr_n. For A=20, the mirror nuclei (6,14) of $(Z,N)^{(p)}=(14,6)$ has two neutrons less than $(Z,N)^{(n)}=(4,16)$. Replacing ^{20}Be by ^{20}C for which r_p=2.55fm and r_n=3.22fm would lead to Δr_p=.92fm>Δr_n=.69fm, which is in agreement with our general results for pairs of mirror nuclei (see subsection 2.3, in particular Fig.1(a)). For the pair (^{20}Si, ^{20}Be), we find that Δr_n is larger than Δr_p, which is also the case for all heavier pairs of extreme isobars.

iii) The fact that Δr_p is smaller than Δr_n for A≥20 is due to the proton confinement produced by the Coulomb barrier, which remains important even at the proton drip line.

A second example of the failure of $A^{1/3}$-laws is given in Fig.1(a), which shows the "surface" $r_n(Z,N)$ for Z≤20 and N≤28. (The few additional results represented by open squares will be discuss later). The top-left hand (bottom-right hand) limit of this surface contains nuclei close to the neutron (proton) drip line or belonging to it. Here, the unadequacy of $A^{1/3}$-laws is obvious in any domain, as small it might be. The important spreading out of r_n along isobar series is clearly shown by the vertical extension of figure 1(a) at any value of A.

2.3 Symmetry properties of the nuclear radii

If the Coulomb effects could be removed, the charge independence of the N-N interaction would imply the following obvious relation

$$r_n(Z,N) = r_p(N,Z) \qquad (4)$$

where the first (second) argument refers to the actual number of protons (neutrons) in the mirror nuclei.

This relation is not valid for heavy nuclei (say A≳100) for which the mirror nucleus (N,Z) of any nucleus (Z,N) stable against particle emission is generally situated far beyond the proton drip line.

In the case of light nuclei, the Coulomb field distrubes only slightly the symmetry relation (4) and our self-consistent HF-BCS approach yields in most cases the following results

$$r_n(Z,N) \lesssim r_p(N,Z) \qquad (5)$$

An illustration of this relation is given in Fig.1(a) where we have added to the two typical sequences of neutron radii

a) the isotope series $r_n(8,N)$, $2 \leq N \leq 22$, and

b) the isotone series $r_n(Z,8)$, $2 \leq Z \leq 18$,

Table 1

Radii of extreme even isobars

In this table, $(Z,N)^{(p)}$ and $(Z,N)^{(n)}$ refer to the first proton-rich (respectively neutron-rich) even isobars which are unstable against proton (neutron) emission (extreme isobars); further, $r_p^{(p)}$ and $r_p^{(n)}$ ($r_n^{(p)}$ and $r_n^{(n)}$) stand for the r.m.s. radii of their proton (neutron) distributions and $\Delta r_p \equiv r_p^{(p)} - r_p^{(n)}$ ($\Delta r_n \equiv r_n^{(n)} - r_n^{(p)}$) gives the corresponding spreading out. A single star indicates a nucleus which is unstable against one nucleon emission while two stars refer to a nucleus which is stable against one nucleon emission but unstable against the emission of a pair of nucleons.

A	$(Z,N)^{(p)}$	$(Z,N)^{(n)}$	$r_p^{(p)}$	$r_p^{(n)}$	Δr_p	$r_n^{(p)}$	$r_n^{(n)}$	Δr_n
10	(8,2)*	(2,8)*	3.85	2.00	1.85	2.00	3.38	1.39
20	(14,6)*	(4,16)**	3.46	2.42	1.04	2.53	3.78	1.25
40	(24,16)*	(10,30)**	3.61	3.02	.59	3.24	4.18	.94
60	(34,26)*	(16,44)*	3.98	3.48	.50	3.67	4.31	.64
80	(44,36)*	(22,58)**	4.27	3.77	.50	4.04	4.95	.91
100	(52,48)*	(28,72)**	4.49	4.11	.38	4.34	4.93	.59
120	(60,60)*	(36,84)**	4.74	4.40	.34	4.64	5.05	.41
140	(68,72)**	(44,96)**	4.95	4.62	.33	4.89	5.46	.57
160	(78,82)*	(46,114)**	5.15	4.82	.33	5.08	5.63	.55
180	(84,96)*	(52,128)*	5.32	5.03	.30	5.31	5.74	.43

the two symmetrical sequences of proton radii (open squares connected by thin lines)

a') the isotone series $r_p(Z,8)$, $3 \leqslant Z \leqslant 18$, and

b') the isotope series $r_p(8,N)$, $2 \leqslant N \leqslant 18$ [+].

The comparison between a) and a') as well as between b) and b' shows the validity of the inequality (5). It is worthwhile to note that the equality in (5) is almost satisfied for $Z \gg N$ whereas the differences $r_p(N,Z) - r_n(Z,N)$ are important for $N \gg Z$. Thus, in the case of light nuclei, the neutron radius of a nucleus close to the proton drip line is practically the same as the proton radius of its mirror which is located in the neighbourhood of the neutron drip line, whereas the proton radius of a nucleus at the proton drip line is significantly larger than the neutron radius of its mirror.

It should be emphasized that the relation (5) supposes that the Coulomb distortion is not strong enough to change the number of bounded orbitals and of quasi-bounded ones (i.e., subbarrier resonances) in mirror nuclei. We have to remember here that in the gap equation, as well as in the pairing correlation term (see Eqs.(51) and (46) of ref.2]), we have extended the summations over all these orbitals. Actually we have encounted a few examples where the above assumption is not verified. For instance, this is the case for the pair of mirror nuclei (10,4) and (4,10). It illustrates typical features of our self-consistent approach, and we shall discuss it in some details.

[+] By reading the arguments of these two additional series on Fig.1(a), do not forget to interchange the labelling of the coordinates.

In ^{14}Ne, the Coulomb field is large enough to push out of the self-consistent potential well the proton orbital 2s1/2, whereas the symmetrical neutron orbital 2s1/2 is just bounded by .16 MeV in ^{14}Be. The proton (neutron) subshells which enter the HF-BCS calculations of ^{14}Ne (^{14}Be) are the following :

1s1/2, 1p3/2, 1p1/2 and 1d5/2 for ^{14}Ne and 1s1/2, 1p3/2, 1p1/2, 1d5/2 and 2s1/2 for ^{14}Be.

Their eigenenergies, r.m.s. radii and pair occupation probabilities are

ε_{jp}=-18.54, -6.92, -1.58 and +3.18 MeV,
r_{jp}= 2.14, 2.94, 3.3a and 4.21 fm,
v^2_{jp}= .9985, .9931, .9525 and .3542 and

ε_{jn}=-22.49, -10.76, -5.15, -.30 and -.16 MeV,
r_{jn}= 2.13, 2.88, 3.15, 4.23 and 7.96 fm,

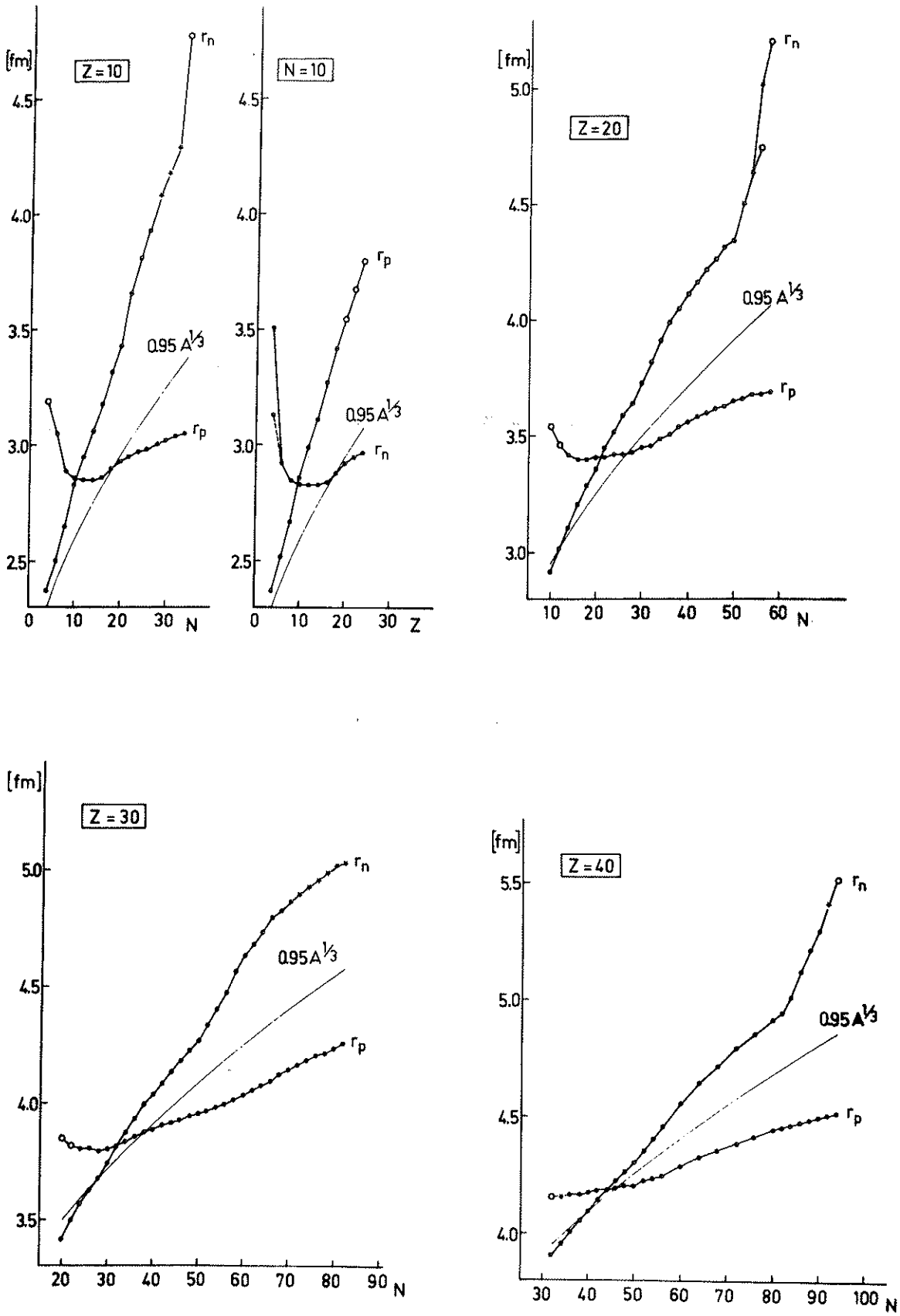

Fig.2 Variation of the r.m.s. radii, r_p and r_n, of the calculated nucleon distributions of the isotopes Z=10, 20, 30, 40 and isotones N=10. Graphical symbols as in fig.4.

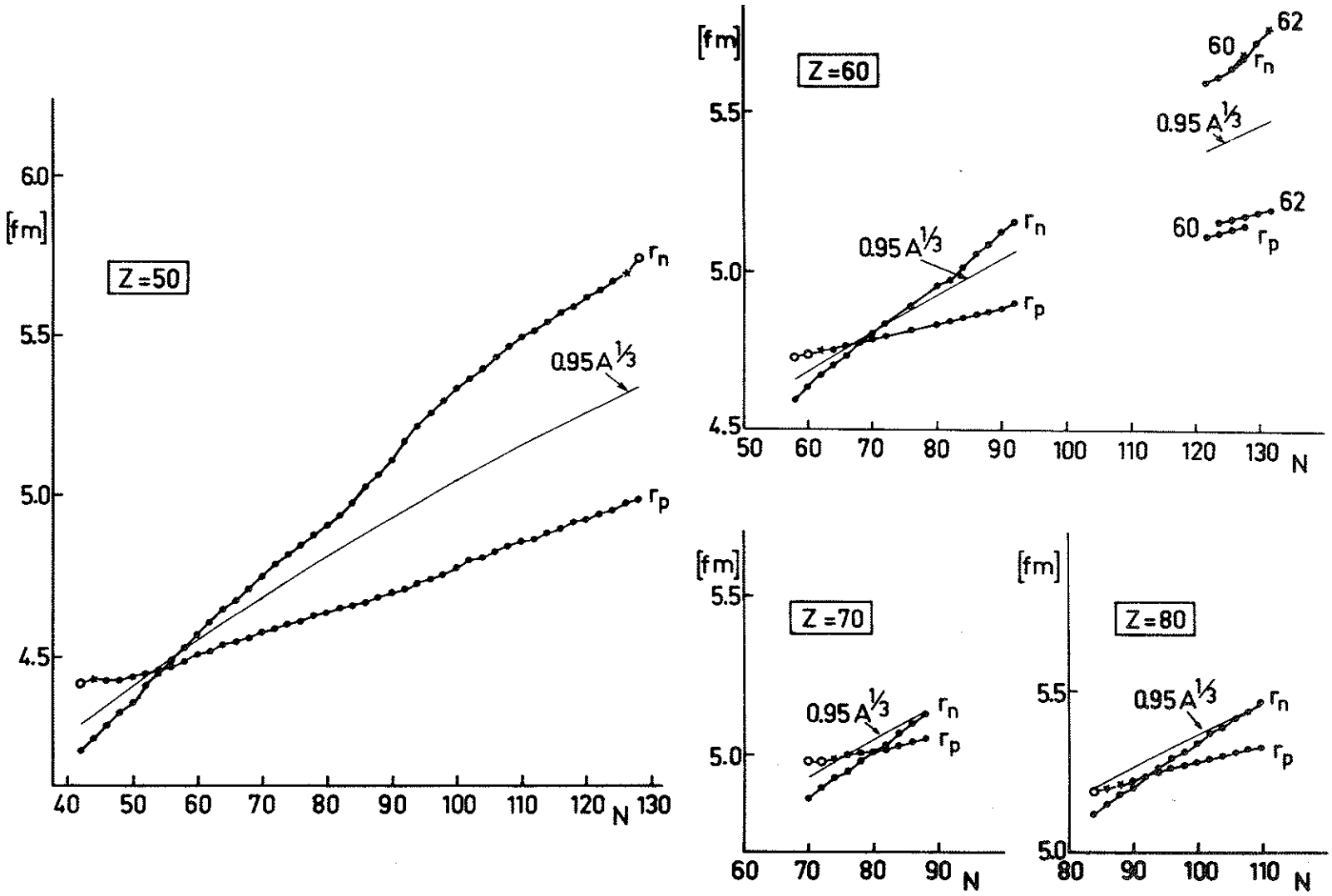

Fig.3 As fig.2 for Z=50, 60, 70 and 80.

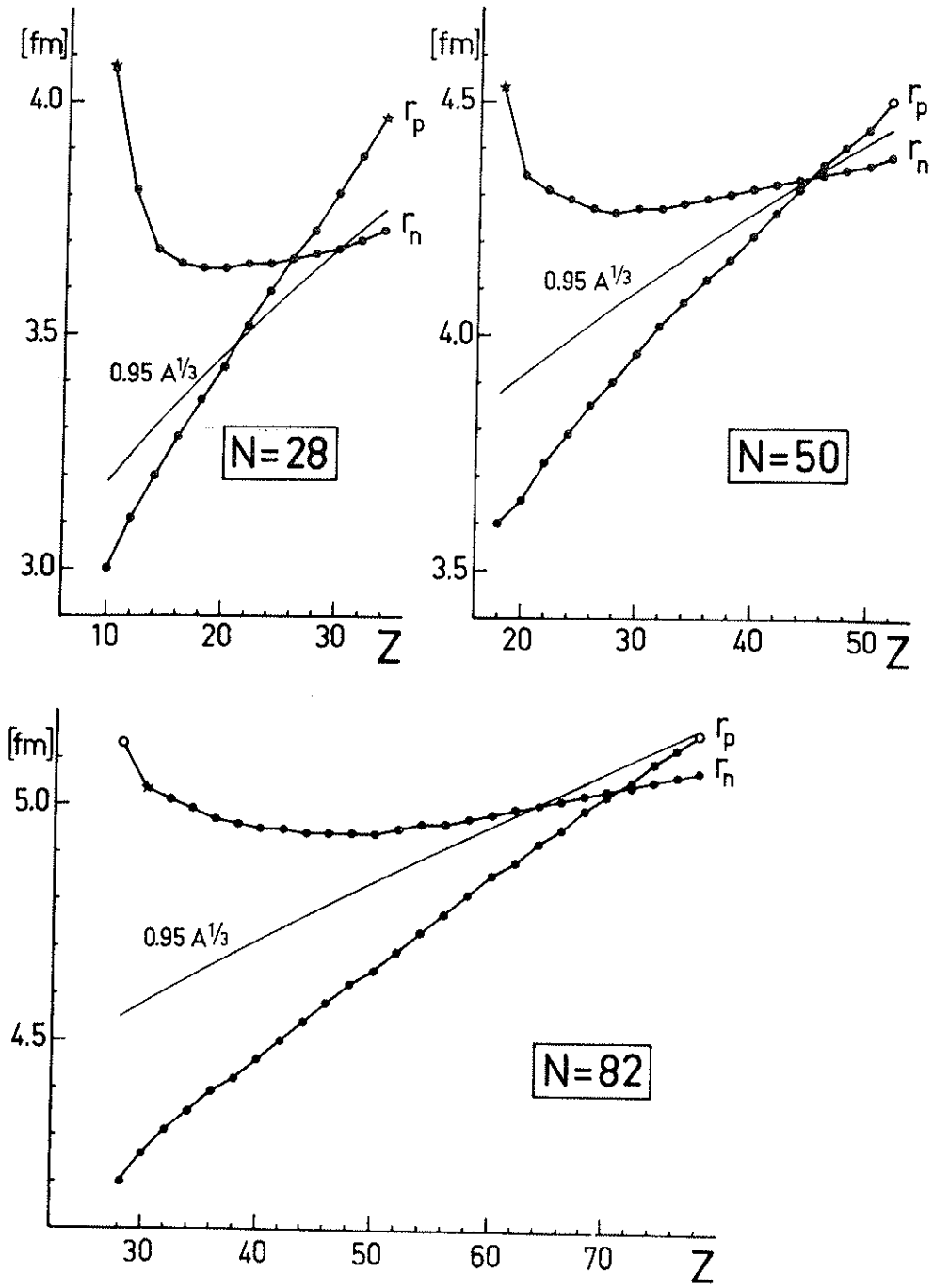

Fig.4 Variation of the r.m.s. radii, r_p and r_n, of the calculated nucleon distributions of the isotones N=28, 50 and 82.

Black circles refer to stable nuclei, open circles to nuclei unstable against one nucleon emission while black stars indicate nuclei unstable against the emission of a pair of nucleon but stable against one nucleon emission.

v^2_{jp}=.9974, .9931, .9520, .2653 and .2684 respectively.

We finally obtain

$r_n(4,10)$=3.510>$r_p(10,4)$=3.189 which violates (5)

$r_n(10,4)$=2.368<$r_p(4,10)$=2.370 which satisfies (5).

If we constrain the neutron 2s1/2 orbital in ^{14}Be to remain unoccupied, the above neutron figures become

ε_{jn}=-22.75, -10.84, -5.29, -.36 and -.20MeV,

r_{jn}= 2.12, 2.88, 3.13, 4.18 and 7.59fm,

v^2_{jn}= .9984, .9930, .9504, .3551 and .0.

In this case, both $r_n(4,10)$=3.126 and $r_p(4,10)$=2.367 satisfy the relation (5) up to the numerical uncertainties. (see also the first points of the isotope (isotone) series Z=10 (N=10) in Fig.2).

An interesting feature of self-consistency, which typically occurs when the saturation property is ensured by a density dependence of the hamiltonian, is the weakening of the binding of low-ℓ orbitals (mainly s and p levels) with the increase of their occupation probabilities [8,+]. In ^{14}Be the binding of the neutron 1s and 2s levels decreases from 22.75 to 22.49 and from .20 to .16 MeV respectively as the occupation probability of the 2s orbital increases from .0 to .27. The r.m.s. radius of this tightly bounded 2s orbital is very large and depends sensitively on small variations of its binding. Such effect brings numerical convergence difficulties for the particular neutron-rich nuclei for which the binding of the last s (or p) orbital, as well as the neutron chemical potential, is close to zero.

2.4 The r.m.s. radii of isotopes and isotones

In order to establish in a systematic way the variations of r_p and r_n against N and Z, calculated values for isotopes and isotones are displayed in Figs.2 to 4. A thin line allows a direct comparison with an $A^{1/3}$-growth of the radii.

In general, at fixed values of Z(N) the neutron (proton) radius increases quasi-monotonically as a function of N(Z). Slope discontinuities are due to shell effects and are, in critical cases, sensitive to the presence (or the absence) in the configuration space of orbitals situated very close to the continuum limit. On the other hand, Z(N) being fixed, the proton (neutron) radius varies between smaller limits in a way which follows from self-consistency.

The proton radius of isotones increases more regularly than the neutron radius of isotopes. This is to be assigned to the Coulomb potential which in addition to the centrifugal barrier confines the proton orbitals situated above the Fermi surface and therefore stabilizes the configuration space.

For isotopes, the increase of r_n in very neutron-rich regions has two typical behaviours according to the way the stability limit of even N isotopes against the emission of a neutron pair is reached with respect to major shell closure. If the drip line occurs just before a closure, the increase of r_n is approximately constant (see Z=50) or reduced (Z=30). This diminishing of the r_n increase before N=82 is responsible for the small value of Δr_n observed at A=120 (see table I). On the other hand, if the stability limit arises after a major shell closure, the increase of r_n is significantly enhanced (see Z=20 and 40). For Z=20, the 3s neutron orbital is unbounded and unoccupied up to N=54. If we constrain it to remain unoccupied, then N=56 becomes a magic number and ^{76}Ca is unstable against one neutron emission (see open circle on the r_n plot at N=56). In fact, we find that the 3s neutron level is bounded for N≥56 and has an occupation probability of .76 and 1.0, and a r.m.s. radius of 11.9 and 11.2 fm in ^{76}Ca and ^{78}Ca respectively. The presence of the 3s neutron orbital in the BCS configuration produces the large value of Δr_n for A=80 (see Table I).

Finally it is interesting to note the actual decrease of $r_p(r_n)$ for Z=10, 20, 30 (any value of N) as one proceeds from the proton (neutron) drip line and adds pair of neutrons (protons), up to the minimal value, which occurs, in light elements, close to the β-stability point. For Z≥40 this effect on r_p is not any more observed.

3. The nuclear Coulomb energy

As shown in section 2, self-consistent calculations predict nuclear size variations which differ sensitively from a $A^{1/3}$-law as one goes away from the β-stability region. A first interesting application concerns the Coulomb energy estimate. For illustrative purpose, the self-consistent total Coulomb energy is compared to values given by liquid-drop-model (LDM) expressions based on a $A^{1/3}$-increase of the proton radius.

For the sake of clarity, the two expressions used here to calculate the Coulomb energy are given below. We restrict ourselves to spherical shapes.

In the energy density method, the Coulomb term reads (see ref.2, Eqs.(16) to (18)) :

$$\varepsilon_c = \frac{1}{2} e \rho_c V_c - .7386 e^2 \rho_c^{4/3}, \qquad (6)$$

where ρ_c represents the charge density associated to the self-consistent proton density. The Coulomb potential $V_c(r)$ is solution of the Poisson equation

$$\Delta V_c(r) = 4\pi e \rho_c(r) \quad . \qquad (7)$$

The second term in (6) corresponds to the statistical treatment of the Coulomb exchange.

+) See in particular Figs. 7,9 and 10 of this reference.

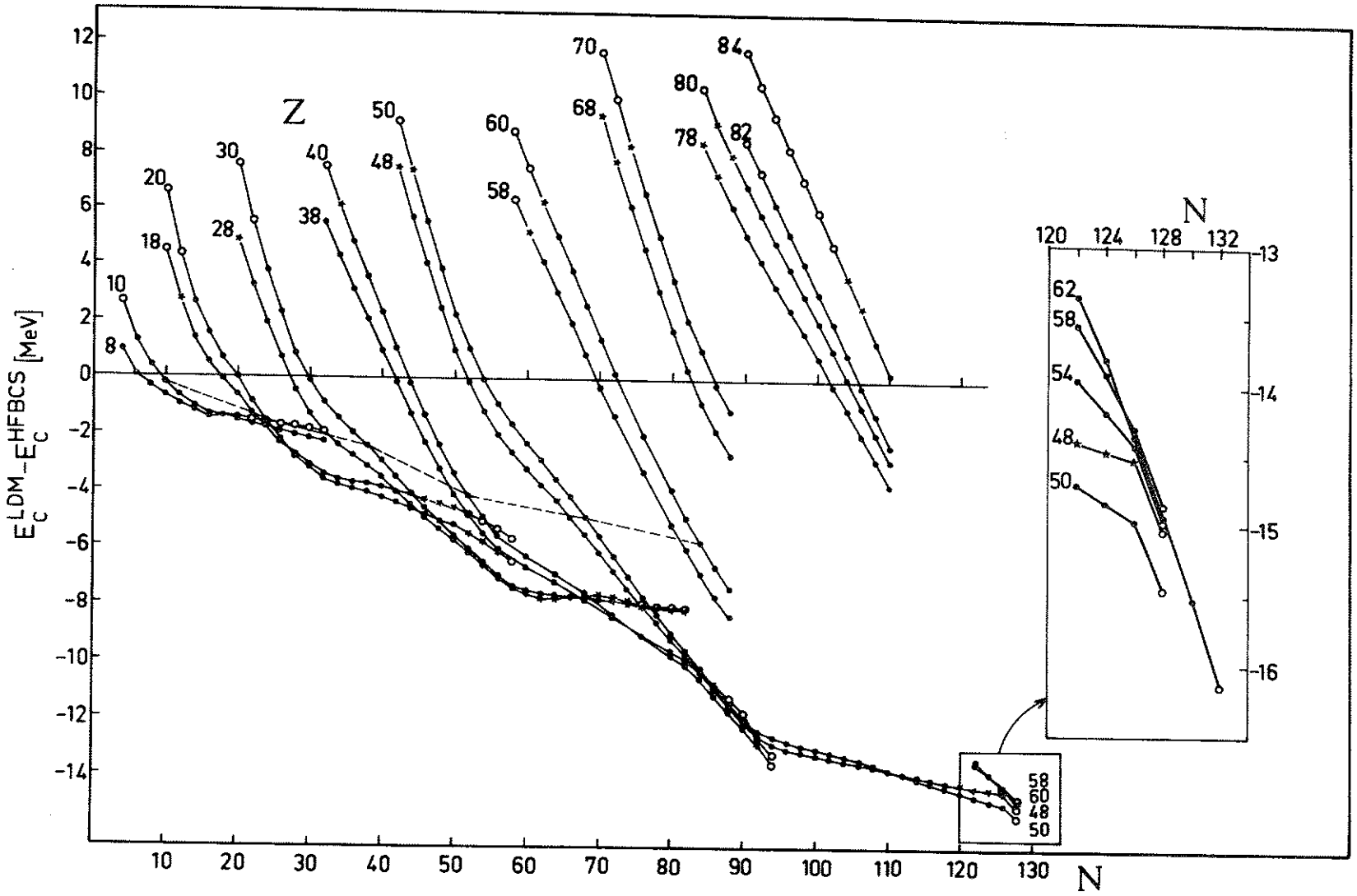

Fig.5 Difference between liquid-drop-model (LDM) and self-consistent (HFBCS) total Coulomb energy for a set of isotope series. Graphical symbols as in fig.4.

As LDM expression, we have chosen the direct and exchange parts [+)] of the Coulomb energy given by Jänecke [9] and used extensively by Seeger and Howard for their calculations of the ground state binding energy of some 8000 nuclei [10]. For spherical shapes, this expression reads :

$$E_c^{LDM}(Z,A)=E_{dir}(Z,R) + E_{exch}(Z,R) \qquad (8)$$

where

$$R=R_0\left\{1+\frac{5}{6}\pi^2\left(\frac{a}{R_0}\right)^2-\frac{7}{24}\pi^4\left(\frac{a}{R}\right)^4\right\},R_0\equiv r_0A^{1/3} \qquad (9)$$

$$E_{dir}(Z,N)=\frac{3}{5}\frac{Z(Z-1)}{R}e^2\cdot\left\{1+c_1\left(\frac{a}{R}\right)^3+c_2\left(\frac{a}{R}\right)^4\right\} \qquad (10)$$

$$E_{exch}(Z,R)=\frac{1}{Z}E_{dir}(Z,R)-3\left(\frac{3}{16\pi}\right)^{2/3}\cdot\frac{e^2Z^{4/3}}{R}\cdot \qquad (11)$$
$$\cdot\left\{1+c_3\left(\frac{a}{R}\right)+c_4\left(\frac{a}{R}\right)^2+c_5\left(\frac{a}{R}\right)^3\right\}$$

The values of the five numerical constants c_1 to c_5 are given in refs. 9] and 10].

The parameter r_0 is fitted on the Coulomb energy of ^{40}Ca calculated in the energy density method. The surface diffuseness parameter is fixed at a=.513fm. The difference $\Delta E_c^{LDM} - \Delta E_c^{HFBCS}$ is plotted in fig.5 against N for 18 values of Z ranging from 8 to 84.

At first glance we see that the differences increase with N, but are contained within a band of -16Mev up to 12Mev. Consequently the effect accounts only for a few percent of the total Coulomb energy. However, the rapid variation of ΔE_c with N and Z is significant. It reaches easily 2Mev for neighbouring isotones with $\Delta Z=2$.

The dotted line indicates the position of β-stable nuclei. It clearly shows that as N increases, the LDM expression has a tendency to underestimate the Coulomb energy. We see also that ΔE_c varies more rapidly on the proton rich- than on the neutron rich-side.

Shell effects are present and modulate the results in two ways. They induce non-monotonic behaviours of ΔE_c along isotope lines, as well as sudden changes between adjacent isotopes, as in the case Z=82-84.

Whether the observed deviations from a simple monotonic variation of the Coulomb energy (as predicted by a $A^{1/3}$-law) may be compensated by ad hoc parametrizations of other components of the LDM formula is dubious. In this respect we note that, in general, the A-dependence of the matter radius r_m follows a $A^{1/3}$-law more closely than r_p and r_n independently. The present results suggest, for instance, that inadequate choices for the variations of r_p against N and Z may lead to unreliable predictions concerning the proton drip line.

[+)] We have omitted the monotonic contribution of the spin-orbit term, which reaches only a few tenths of a percent of the total Coulomb energy.

References

[1] W. Kohn, Nobel Symposium on Collective Properties of Physical Systems, Ed. by B. Lundqvist and S. Lundqvist, Academic Press (New York and London) (1973) p. 154 and quoted references.

[2] M. Beiner and R.J. Lombard, Ann. of Phys. (NY) 86 (1974) 262

[3] M. Beiner, R.J. Lombard and D. Mas, Atomic Data and Nucleus Data Tables 17 (1976) to be published

[4] Atomic Data and Nuclear Data Tables 14 (1974) 489

[5] J.P. Auger, to be published

[6] Apart from results quoted in refs.2] and 5], see for instance:
X. Campi, Nuclear Self-consistent Fields, Ed. by G. Ripka and Porneuf, North-Holland/American Elsevier (1975) 271
J.L. Friar and J.W. Negele, Adv. in Nucl. Phys. 8 (1975) 219

[7] A.H. Wapstra and N.B. Gove, Nucl. Data Tables 9 (1971) 265

[8] M. Beiner, R.J. Lombard and D. Mas, Nucl. Phys. A249 (1975) 1

[9] J. Jänecke, Nucl. Phys. A181 (1972) 49

[10] P.A. Seeger and W.M. Howard, LA 5750, UC-34c (Oct. 1974).

Note added :
The fig.1b was first published in Annals of Physics ref. 2]. It is reproduced here with permission.